Distinguishing ichthyogenic turbulence from geophysical turbulence

Citation	Pujiana, K., Moum, J. N., Smyth, W. D., & Warner, S. J. (2015). Distinguishing ichthyogenic turbulence from geophysical turbulence. Journal of Geophysical Research: Oceans, 120(5), 3792-3804. doi:10.1002/2014JC010659
DOI	10.1002/2014JC010659
Publisher	John Wiley & Sons Ltd.
Version	Version of Record
Terms of Use	http://cdss.library.oregonstate.edu/sa-termsofuse

AGU PUBLICATIONS

JGR

Journal of Geophysical Research: Oceans

RESEARCH ARTICLE
10.1002/2014JC010659

Special Section:
The 2011-12 Indian Ocean Field Campaign: Atmospheric-Oceanic Processes and MJO Initiation

Distinguishing ichthyogenic turbulence from geophysical turbulence

Kandaga Pujiana[1,2], James N. Moum[1], William D. Smyth[1], and Sally J. Warner[1]

[1]College of Earth, Ocean, and Atmospheric Sciences, Oregon State University, Corvallis, Oregon, USA, [2]Faculty of Earth Sciences and Technology, Institut Teknologi Bandung, Bandung, Indonesia

Abstract Measurements of currents and turbulence beneath a geostationary ship in the equatorial Indian Ocean during a period of weak surface forcing revealed unexpectedly strong turbulence beneath the surface mixed layer. Coincident with the turbulence was a marked reduction of the current speeds registered by shipboard Doppler current profilers, and an increase in their variability. At a mooring 1 km away, measurements of turbulence and currents showed no such anomalies. Correlation with the shipboard echo sounder measurements indicate that these nighttime anomalies were associated with fish aggregations beneath the ship. The fish created turbulence by swimming against the strong zonal current in order to remain beneath the ship, and their presence affected the Doppler speed measurements. The principal characteristics of the resultant ichthyogenic turbulence are (i) low wave number roll-off of shear spectra in the inertial subrange relative to geophysical turbulence, (ii) Thorpe overturning scales that are small compared with the Ozmidov scale, and (iii) low mixing efficiency. These factors extend previous findings by Gregg and Horne (2009) to a very different biophysical regime and support the general conclusion that the biological contribution to mixing the ocean via turbulence is negligible.

Key Points:
- Ichthyogenic turbulence is diagnosed from acoustics and turbulence measurements
- Small, turbulent eddies with low mixing efficiency characterize ichthyogenic turbulence
- Contribution to ocean dynamics is negligible

Correspondence to:
J. N. Moum,
moum@coas.oregonstate.edu

Citation:
Pujiana, K., J. N. Moum, W. D. Smyth, and S. J. Warner (2015), Distinguishing ichthyogenic turbulence from geophysical turbulence, *J. Geophys. Res. Oceans*, *120*, 3792–3804, doi:10.1002/2014JC010659.

Received 18 DEC 2014
Accepted 21 APR 2015
Accepted article online 25 APR 2015
Published online 29 MAY 2015

1. Introduction

The detection of enhanced temperature and velocity microstructure in association with acoustic backscatter measurements indicating the recent presence of swimming fish schools [*Farmer et al*., 1987] clearly showed the existence of biogenic turbulence in the ocean. Concerns about the potential contribution of biogenic turbulence to mixing the stratified ocean were succinctly summarized by *Katija* [2012].

Kunze et al. [2006] showed a large increase in turbulence attributed to daily upward migration of an acoustic backscatter layer composed of up to 10^4 krill individuals per cubic meter in Saanich Inlet, British Columbia, Canada. Based on this finding and the global abundance of krill, they suggested that turbulence production due to swimming marine organisms might be significant or comparable to that due to breaking internal gravity waves. This inference was later revised with the addition of open ocean measurements and the recognition that turbulence bursts in krill aggregations in the inlet occurred infrequently and could not efficiently mix the ocean [*Rousseau et al*., 2010].

Measurements by *Gregg and Horne* [2009] in Monterey Bay, California provided a measure of the efficiency of mixing within schooling fish relative to that due to geophysical sources. They identified several unique features of the fish-generated (*ichthyogenic*) turbulence. Most significantly, while the turbulence kinetic energy dissipation rate (ϵ) within fish aggregations was $\sim$100 times greater than its background value, the mixing efficiency (Γ) was $\sim$100 times smaller. The diapycnal buoyancy flux, $\Gamma\epsilon$, was therefore indistinguishable from its background value, i.e., the ichthyogenic component was negligible. This conclusion was countered by *Lorke and Probst* [2010] who found Γ within fish shoals to be no different from that away from the shoals.

Recent turbulence profiling measurements in the equatorial Indian Ocean as part of the Dynamics of the Madden-Julian Oscillation experiment (DYNAMO) [*Yoneyama et al*., 2013; *Moum et al*., 2014] revealed high nocturnal ϵ coincident with fish aggregations revealed by simultaneous acoustic backscatter measurements from a high-frequency echo sounder (120 kHz). Multiple acoustic Doppler current profilers (ADCPs) revealed an apparent decrease in mean current speed, and an increase in speed variance, in the presence of nighttime fish aggregations. In other words, the measured velocity was sporadically altered so as to become closer to the ship's velocity (zero, in the Earth's reference frame), suggesting that the ADCPs were frequently

measuring the swimming velocity of ship-following fish. Velocity and turbulence measurements at a nearby mooring (within 1 km) indicated no coincident high ϵ values, and no apparent decrease in mean current speed or increase in speed variance.

In this paper we demonstrate the nature of the fish aggregations as revealed by the shipboard acoustic measurements. We also demonstrate the localization of the fish through the absence of similar properties at the nearby mooring. Finally, we document the measurable properties of ichthyogenic turbulence that contrast it with turbulence generated by geophysical processes. Those properties are (1) reduced inertial subrange in turbulent shear spectra; (2) increased Ozmidov (or buoyancy) length scale relative to Thorpe scale; and (3) low mixing efficiency.

We propose that these properties result from the small size and high energy of turbulent eddies generated by fish compared to those generated through geophysical instabilities. The third property, together with the local or infrequent nature of fish aggregations, indicates the minimal effect that ichthyogenic turbulence has on ocean mixing. These findings verify the results of *Gregg and Horne* [2009] but here using a far more comprehensive set of measurements, in a very different geophysical flow regime, and for fish swimming at a large and relatively constant velocity. Our findings disagree with those of *Lorke and Probst* [2010].

Specifications of the shipboard and moored measurements used in this study are given in section 2. In section 3, we describe and compare measurements of currents and turbulence obtained from those two platforms. Distinguishing characteristics of ichthyogenic turbulence are identified in section 4. In section 5, we discuss likely explanations for the observed fish behavior and of the ichthyogenic turbulence. Conclusions are summarized in section 6.

2. Data

2.1. Shipboard Data

The R/V *Roger Revelle* was stationed at 0°N and 80.5°E almost continuously during October to early December 2011 to record time series of oceanic and atmospheric variables in connection with studies of the Madden-Julian Oscillation (MJO). *Revelle* has dynamic positioning capabilities and, excepting a few excursions for various reasons (including attempts to avoid fish aggregations), maintained a geostationary position throughout. Here we discuss subsets of data from multiple hull-mounted ADCPs, a BioSonics DTX 120 kHz echo sounder, and the *Chameleon* microstructure profiler during 21 November to 2 December 2011, a period during which both suppressed and active phases of the MJO were observed [*Moum et al*., 2014].

ADCP data were collected at 75 kHz (8 m resolution), 140 kHz (3 m resolution), and 150 kHz (4 m resolution). The data we analyze for this study are profiles of velocity, acoustic reflectivity, and vertical shear. A hull-mounted echo sounder measured acoustic backscatter at 120 kHz with a vertical resolution of 0.01 m and the backscatter data were calibrated as volume backscattering strength S_v (dB).

The *Chameleon* microstructure profiler collected a total of 1820 microstructure profiles over the period of 21 November to 2 December 2011 at nominal descent rates (w) of 0.9–1.0 m s^{-1}. Shear probes on *Chameleon* were sampled at 204 Hz. Assuming Taylor's frozen flow approximation, the turbulence shear profile was estimated as $du/dz = wdu/dt$, broken into half-overlapping 1 m intervals, Fourier transformed, and then fit iteratively to a universal spectrum [*Nasmyth*, 1970] in order to obtain the integrated shear variance, $\overline{(du/dz)^2}$ [*Moum et al*., 1995]. We then estimated $\epsilon = 7.5\nu\overline{(du/dz)^2}$, where ν is the kinematic viscosity of seawater and isotropy is assumed.

2.2. Moored Data

The *R/V Revelle* was stationed within 1 km of a surface mooring at 0°N and 80.5°E, a component of the Research Moored Array for African-Asian-Australian Monsoon Analysis and Prediction (RAMA) [*McPhaden et al*., 2009]. Current measurements from an upward-looking ADCP are averaged into 1 h, 5 m depth bins. In addition, we investigate temperature microstructure data from a χpod attached to the RAMA mooring at 59 m depth. χpod sampled temperature at 10 Hz and its analog time derivative T_t at 120 Hz using fast thermistors [*Moum and Nash*, 2009]. Using the spectral fitting methods described by *Moum and Nash* [2009], we estimated the dissipation rate of temperature variance, χ_T, and the turbulent kinetic energy dissipation rate, ϵ_χ. The principal assumptions that underlie this estimate are (i) the turbulence is isotropic at high wave

numbers, (ii) the energy-containing eddies are statistically stationary and homogeneous, (iii) the turbulent diffusivities of heat and mass are equal, and (iv) Γ has the constant value of 0.2. For further details see *Osborn and Cox* [1972], *Osborn* [1980], and *Moum and Nash* [2009]. Assumptions (i)–(iii) will be justified retroactively in section 5.2. The fourth assumption is questionable as there are demonstrated deviations from a constant value of Γ [*Smyth et al*., 2001], including the example of ichthyogenic turbulence discussed here. However, the dependence of χ_T on Γ is weak and of ϵ is linear; implications are discussed in section 5.2.

3. Acoustic and Microstructure Measurements

3.1. Overview

During late November and early December 2011, an active-phase MJO event propagated eastward across the tropical Indian Ocean [*Moum et al*., 2014]. A strong westerly wind burst (WWB-1) associated with this event passed our location beginning on 24 November (Figure 1a), followed by a similar event (WWB-2) beginning on 27 November. Prior to this, the suppressed phase of the MJO was characterized by weak zonal wind stress, strong shortwave radiation, and stabilizing surface buoyancy flux (Figures 1a–1c). During the WWBs, winds were elevated, shortwave radiation was reduced and the surface buoyancy flux was destabilizing. The upper ocean responded to the WWBs through the generation of a Yoshida-Wyrtki jet, whose signature was evident in the initial acceleration of upper ocean currents and subsequent sustained currents in the upper 75 m (Figures 1d and 1e).

Although both shipboard and moored ADCPs generally captured the passage of the Yoshida-Wyrtki jet, the details of the jet as measured by the two ADCPs are far from identical (Figures 1d and 1e). For example, within the first 12 h following the onset of WWB-1 on 24 November, the shipboard ADCP registered accelerations only above 25 m, whereas the moored ADCP showed acceleration down to 50 m depth (compare Figures 2a and 2b). After the first 12 h following onset, both ADCPs detected the accelerated current.

The discrepancy in the ADCP signals can be resolved if one assumes that the *Revelle's* ADCP was registering some combination of the true current $\vec{U}$ and the velocity of the fish, $\vec{U}_{fish}$. Suppose that this combination is linear, i.e.,

$$\vec{U}_{Revelle} = \vec{U}(1-R) + \vec{U}_{fish}R, \tag{1}$$

where R is the ichthyogenic fraction of the ADCP signal. For fish swimming to keep pace with a geostationary ship, $\vec{U}_{fish}=0$, and therefore $R=(|\vec{U}|-|\vec{U}_{Revelle}|)/|\vec{U}|$. We assume (and will later confirm) that the ADCP mounted on the nearby RAMA mooring was free of fish effects, so that its output $\vec{U}_{RAMA}$ equaled the true velocity $\vec{U}$. Based on these assumptions, we define R as

$$R = \frac{|\vec{U}_{RAMA}| - |\vec{U}_{Revelle}|}{|\vec{U}_{RAMA}|}. \tag{2}$$

Averaged over 20–80 m, R showed a distinct diurnal variation, with consistently positive values at night (compare Figures 1f and 1b). Daytime values were more variable. Negative values suggest that R can be influenced by nonbiological factors such as lateral current variability and measurement errors. All of these factors were magnified in the suppressed phase, when the true current was relatively weak and therefore the denominator of (2) was small.

A discrepancy between shipboard and moored measurements was also observed in ϵ. Periodic amplifications of ϵ are evident in the microstructure profiler-derived data but not in the moored data, and this signal was most pronounced during the suppressed phase of the MJO preceding 24 November (Figure 1g). The large nighttime values occurred below the base of the surface mixed layer, and could not have resulted from surface forcing as the winds were weak and the observed dissipation rate was an order of magnitude greater than the air-sea buoyancy flux due to convective cooling (Figures 2c and 2d). During times of enhanced S_v beneath the ship, ϵ values from the shipboard microstructure profiler were typically 10 times larger than those measured at the mooring (Figures 1g, 1h, 2c, and 2e). High near-surface values of S_v observed during the wind bursts are associated with bubble clouds created by breaking waves.

Both the reduction of $|\vec{U}_{Revelle}|$ and the increase of ϵ during dark hours coincided with amplification of S_v (Figures 1h and 2e). Below about 20 m depth, S_v varied diurnally, with large values during the night (13:00–24:00 UTC) and much smaller values during the day (01:00–13:00 UTC). Over the complete

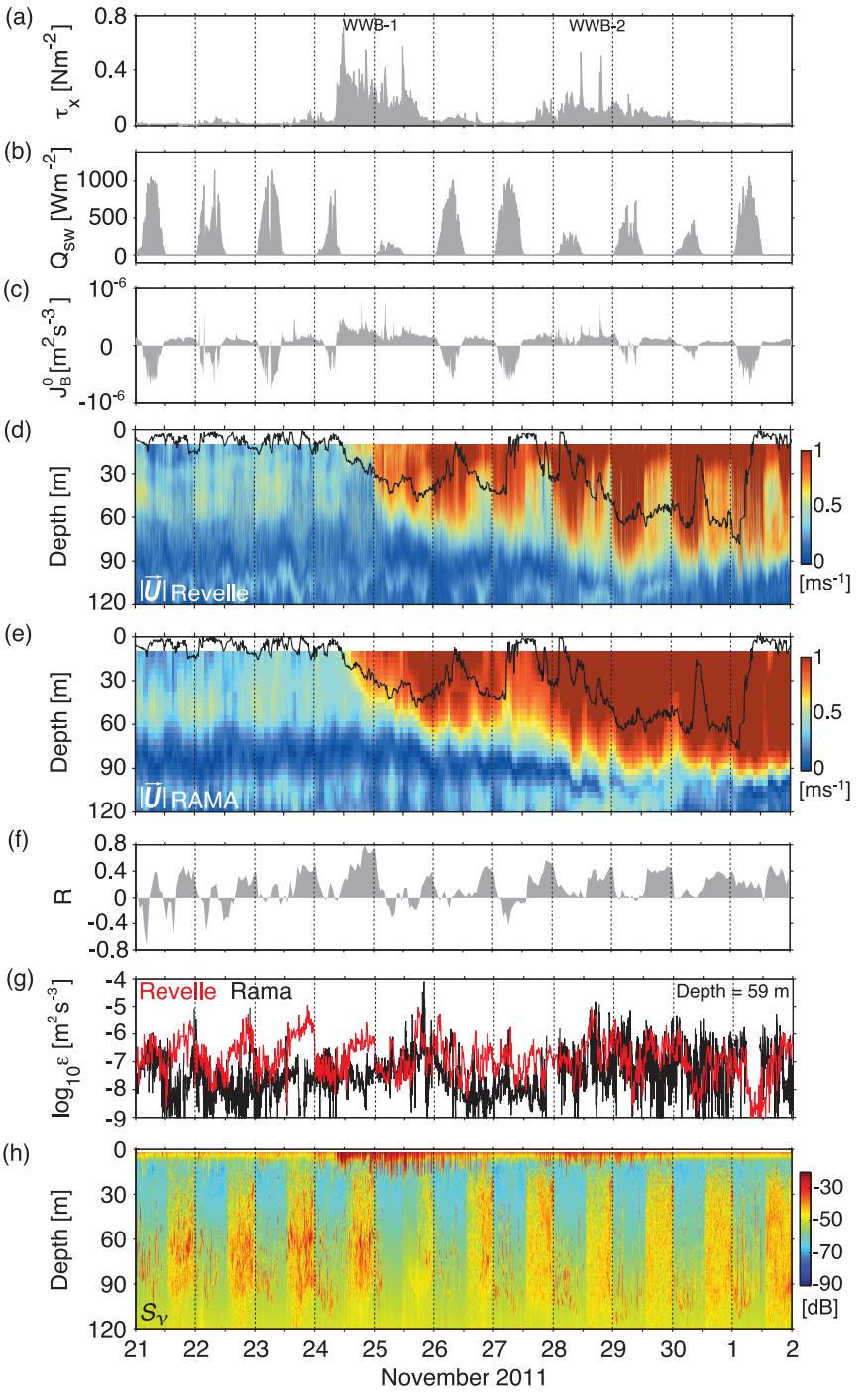

Figure 1. Time series at 0°N and 80.5°E during 21 November to 2 December 2011. (a) Zonal wind stress. Values >0 indicate eastward wind stress. Two westerly wind bursts [WWBs] were observed. (b) Shortwave radiation Q_{SW}. Values >0 indicate daytime hours. (c) The variation of the surface buoyancy flux. Values >0 (<0) indicate surface cooling (heating). (d) Zonal current from R/V *Revelle* ADCP (150 kHz). (e) Zonal current from a nearby RAMA buoy. Black contour in Figures 1d and 1e illustrates the mixed-layer depth. (f) The ichthyogenic fraction of the ADCP signal averaged between 20 and 80 m. (g) Turbulent kinetic energy dissipation rates observed by a moored *χpod* recorder (black) and the *Chameleon* turbulence profiler (red). The moored data illustrate ϵ at 59 m, and the profiler data show vertical averages over 55 to 63 m. (h) Volume backscattering strength S_v.

interval 21 November to 2 December, the probability density function of S_v during nighttime differed significantly from that during the day (Figure 3a). The average nighttime S_v was -47 ± 3 dB, significantly larger than average daytime S_v of -58 ± 3 dB.

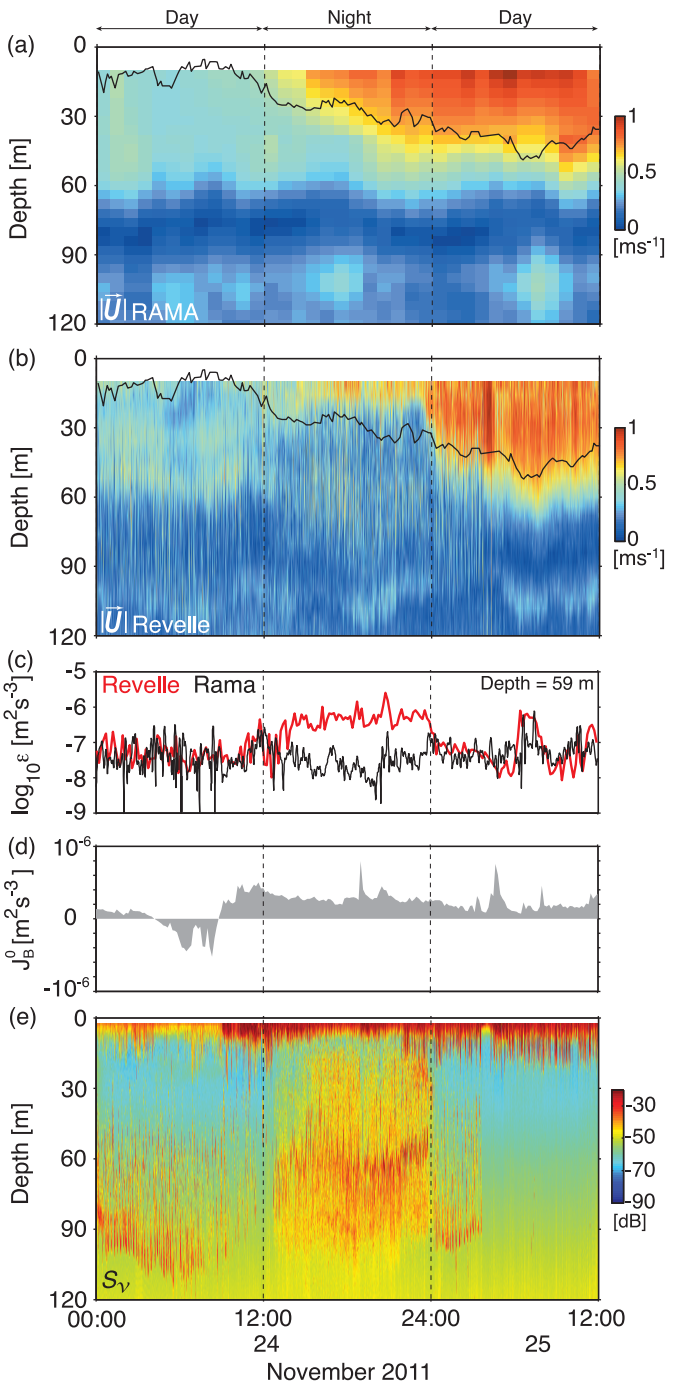

Figure 2. Time series of (a) RAMA ADCP speed, (b) R/V *Revelle* ADCP (150 kHz) speed, (c) moored (black) and shipboard (red) turbulence dissipation rates, (d) surface buoyancy flux, and (e) volume backscattering strength at 0°N and 80.5°E on 24–25 November 2011. Black contour in Figures 2a and 2b indicates the mixed-layer depth.

Our impression that the fish were following the ship is further supported by differences in acoustic backscatter registered by the individual beams of the ADCP. The forward and aft beams registered significantly different distributions of S_v, with means differing by ~6 dB (Figure 3b).

3.2. Current Speed Variability

Depth-dependent profiles of $|\vec{U}_{RAMA}|$ and $|\vec{U}_{Revelle}|$ taken during daytime were identical within 95% bootstrap confidence limits (Figure 4a, orange curves). Also, the mean profile of $|\vec{U}_{RAMA}|$ taken at night (dashed black curve) was not significantly different from the daytime profile. In contrast, the mean nighttime profile of $|\vec{U}_{Revelle}|$ (solid black curve) differed significantly, particularly for speeds measured over depths 20–80 m. The mean ichthyogenic fraction of the ADCP signal was 0.2–0.3 between 40 m and 70 m, declining steeply below that layer and more gently above (Figure 4b).

Both moored and shipboard ADCP speeds exhibit bimodal probability distributions corresponding to the suppressed and active MJO phases, the latter dominated by the larger speeds characteristic of the Yoshida-Wyrtki jet (Figure 5a). Distributions of daytime and nighttime $|\vec{U}_{RAMA}|$ and daytime $|\vec{U}_{Revelle}|$ were very similar, whereas the distribution of the nighttime shipboard ADCP (solid, black curve) was dramatically different. This vivid day/night difference, together with the absence of any difference at the mooring, confirms our earlier assumption that fish effects were strongly localized near the *Revelle* while the moored ADCP measured the true current (section 3.1).

The distributions indicate that the nighttime speed shift between the moored and shipboard ADCPs was larger during the active MJO phase. In the depth range 20–80 m, the mean nighttime speed shift during the suppressed and active phases varied by -0.10 ± 0.01 m s^{-1} and -0.32 ± 0.03 m s^{-1}, respectively. This variation is consistent with the observation that nighttime values of R varied little between phases (Figure 1f) and showed no indication of bimodality (Figure 5b). Day/night distributions of R were also distinctly different (Figure 5b), with daytime mean indistinguishable from zero and nighttime values distributed about 0.3.

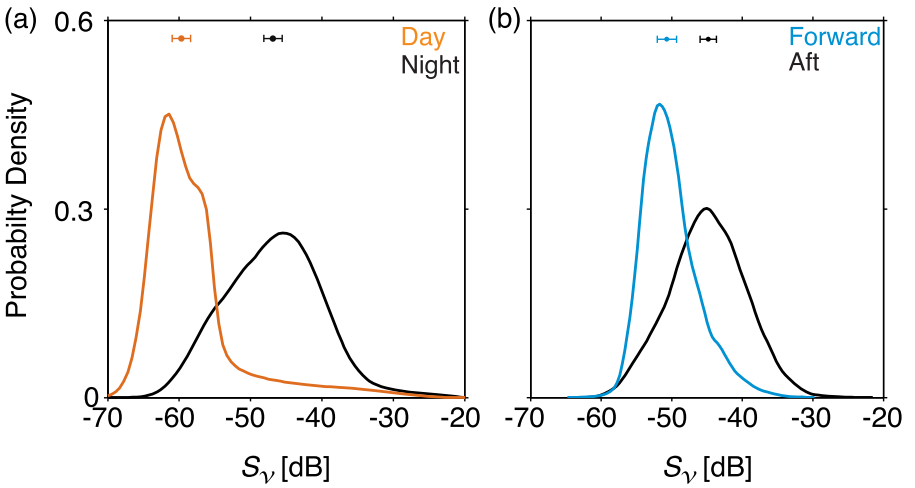

Figure 3. (a) Probability density functions of S_v during daytime (orange) and nighttime (black) measured by the *Revelle* echo sounder. Orange (black) circle indicates the mean of S_v during daytime (nighttime), and error bars denote the 95% bootstrap confidence limits. (b) Probability density functions of S_v during nighttime acquired by the *Revelle* ADCP (150 kHz) beams oriented toward the bow (cyan) and stern (black) of the ship. Cyan (black) circle indicates the mean of S_v during nighttime at the bow (stern), and error bars denote the 95% bootstrap confidence limits. The data were observed between 20 and 80 m over 21 November to 2 December 2011.

Nighttime also brought increased variance in $|\overrightarrow{U}_{Revelle}|$ (1 h variance from 5 s ensemble averages), with variance >0.01 m^2 s^{-2} occurring more frequently during nighttime (Figure 5c). This elevated variance is consistent with our impression that measurements taken at night represent a combination of the very different velocities of the water and the fish.

3.3. Turbulence Variability

At the *Revelle*, intense turbulent dissipation ($\epsilon > 5 \times 10^{-7}$ m^2 s^{-3}) was observed during nighttime over the MJO suppressed phase, extending for tens of meters beneath the surface mixed layer (Figure 6a). This signature became less distinct with the onset of WWB-1. High ϵ values are also evident in the strongly sheared layer at the base of the Yoshida-Wyrtki jet during the active phase (Figures 6a and 6b).

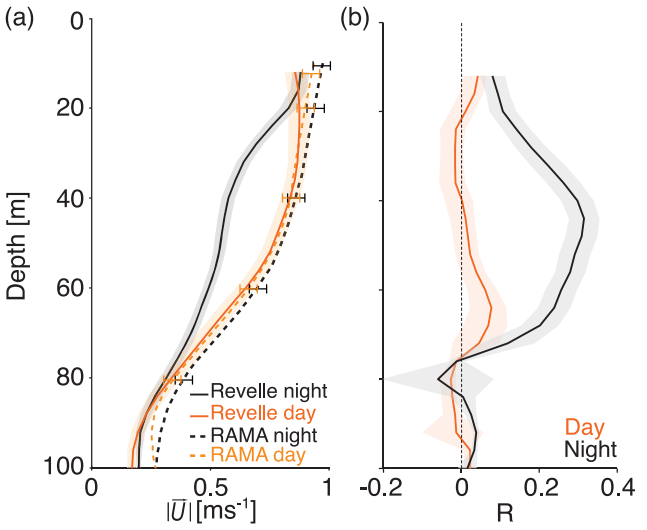

Figure 4. (a) Profiles of mean speed during daytime (orange) and nighttime (black) observed from R/V *Revelle* ADCP (150 kHz) (solid curves) and RAMA buoy (dashed curves). The 95% bootstrap confidence limits are given as error bars (RAMA) and shaded bar (*Revelle*). (b) Profile of R during daytime (orange) and nighttime (black). The 95% bootstrap confidence limits are given as shaded bar. The speed and R are averaged over 21 November to 2 December 2011.

Strong nighttime turbulence coincided with biological aggregations as inferred from S_v (Figure 6c). Aggregations were not observed during daytime. During the suppressed phase, nighttime ϵ exceeded daytime ϵ by a factor of 7 (averaged over 20–80 m and from 21 to 24 November; solid curves in Figure 7).

Nighttime values of ϵ and S_v were correlated, with squared correlation coefficient $r^2 = 0.81$, whereas the correlation between ϵ and S_v during daytime was not significantly different from zero (Figure 8). During daytime, shear likely accounts for enhanced dissipation rates at depths of 20–80 m, as ϵ within that depth range was correlated to squared shear with $r^2 = 0.58$ during the suppressed phase.

The moored microstructure recorders, despite being deployed within 1 km of the *Revelle*, did not record a nighttime bias in turbulent dissipation (Figure 7,

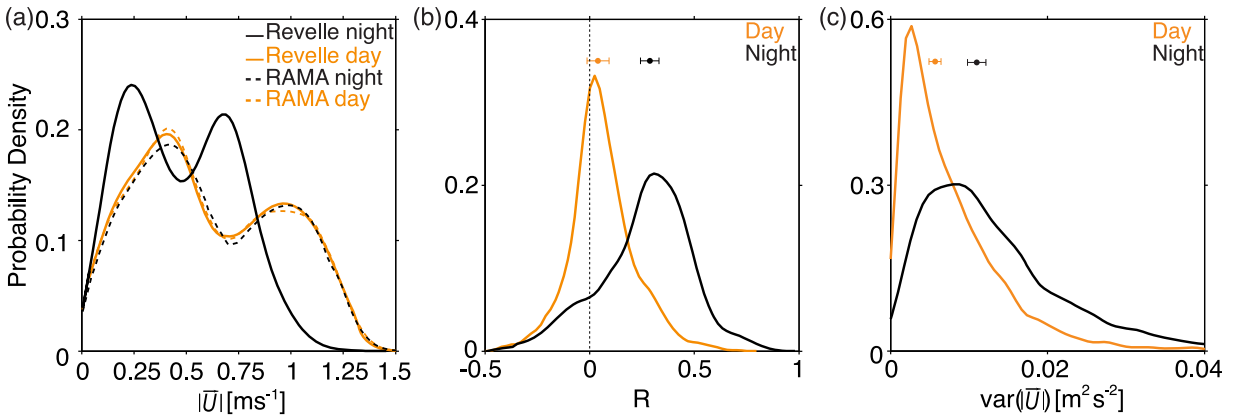

Figure 5. (a) Probability density functions of R/V *Revelle* ADCP (150 kHz) speed (solid curves) and RAMA ADCP speed (dashed curves) observed during daytime (orange) and nighttime (black). (b) Probability density functions of R observed during daytime (orange) and nighttime (black). (c) Probability density functions of speed variance during daytime (orange) and nighttime (black) from the R/V *Revelle* ADCP (150 kHz). The data were acquired at depth range 20–80 m from 21 November to 2 December 2011. Colored circles indicate the mean of the data during daytime (orange) and nighttime (black) respectively, and error bars denote the 95% bootstrap confidence limits.

dashed curves). This suggests that the effect of biological aggregations on turbulence, like the effect on ADCP current readings, occurred locally beneath the vessel.

4. Distinguishing Features of Ichthyogenic Turbulence

We have defined ichthyogenic turbulence to be the result of acoustically observed aggregations beneath the ship. We understand geophysical turbulence to be characterized by a wave number spectrum of velocity shear (as measured by shear probes) with a broad inertial subrange of slope $k^{1/3}$, to have overturning

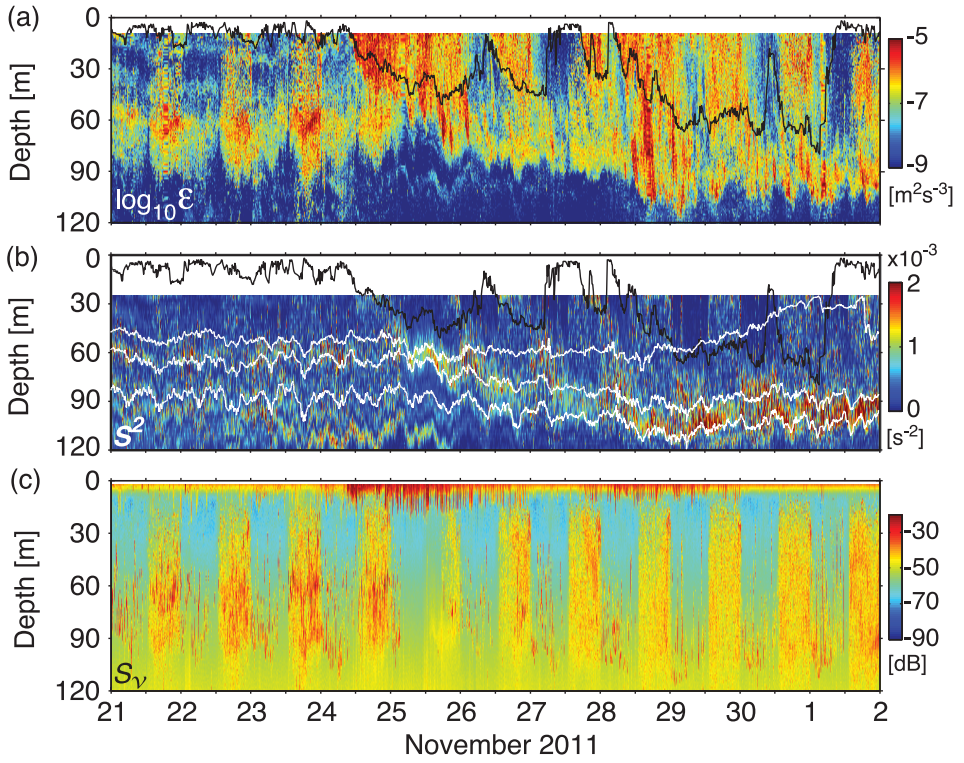

Figure 6. Time series at 0°E and 80.5°E during 21 November to 2 December 2011. (a) Turbulence dissipation rates from the *Chameleon* microstructure profiler. (b) Squared shear S^2 from the R/V *Revelle* ADCP (140 kHz). Black contour indicates the mixed-layer depth, while white contours show isopycnals of 1022.6, 1023, and 1024 kg m^{-3}. (c) Volume backscattering strength S_v.

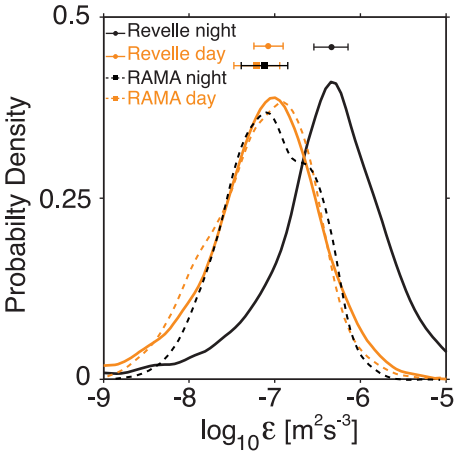

Figure 7. Probability density functions of ϵ from the *Chameleon* microstructure turbulence profiler (solid curves) measured at depths of 55–64 m and from a moored χpod recorder (dashed curves) at 59 m during daytime (orange) and nighttime (black) over 21–24 November 2011. Colored circles and rectangles indicate the mean ϵ from *Chameleon* and χpod, respectively. Error bars denote the 95% bootstrap confidence limits.

(Thorpe) length scale (L_T) roughly equal to buoyancy (Ozmidov) scale (L_O) [*Dillon*, 1982], and to have a mixing efficiency (Γ) close to 0.2 [*Moum*, 1996a; *Smyth et al.*, 2001]. To demonstrate the distinction between ichthyogenic turbulence and geophysical turbulence, we focus on the suppressed phase preceding WWB-1 and the depth range 55–85 m, as this regime most clearly shows the day/night differences associated with the fish aggregations.

4.1. Low Wave Number Departure of Turbulence Spectra From Inertial Subrange

To examine the effect on spectra of small-scale vertical gradients of horizontal velocity ($\Phi_{(u_z)}$), as measured by shear probes on *Chameleon*, we select data from the depth range 55–85 m during both daytime and nighttime. These were further selected according to $S_v > -45$ dB and $9 \times 10^{-7} < \epsilon < 3 \times 10^{-6}$ m^2 s^{-3} (nighttime) and $S_v < -52$ dB and $1 \times 10^{-7} < \epsilon < 5 \times 10^{-7}$ m^2 s^{-3} (daytime). Each of these yielded 46 individual spectra, which were then averaged dimensionally (Figure 9a). Each individual spectrum was further nondimensionalized by Kolmogorov scalings and reaveraged (Figure 9b). While spectra at $k > 1$ cpm are in reasonable agreement with the empirical turbulence spectrum of *Nasmyth* [1970], the ichthyogenic turbulence spectrum trends steeply downward toward smaller k for $k < 1$ cpm, deviating from the Nasmyth spectrum at the lowest values of k. This change is significant at the 95% confidence level.

4.2. Increased L_O

Vertical profiles of L_T did not differ significantly between night and day (Figure 10a, gray and yellow curves). Daytime profiles (yellow and red curves) gave $L_O \simeq 0.8 L_T$, as has been frequently found to be typical of geophysical turbulence from observations in thermoclines [*Moum*, 1996b]. In contrast, nighttime profiles of L_O (Figure 10a, black) revealed values exceeding L_T (grey) by factors of 2–3. Probability density functions show that nighttime values of L_O/L_T were heavily skewed toward large values (Figure 10b).

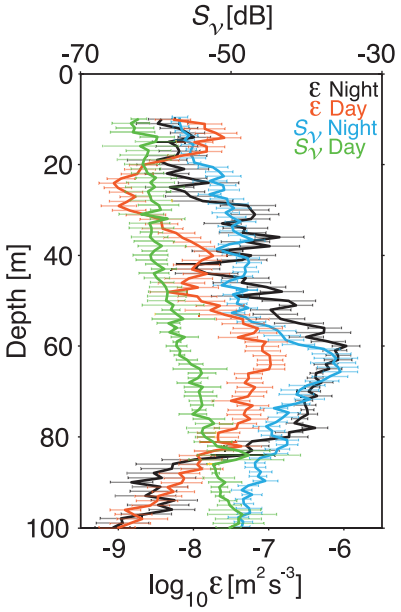

Figure 8. Profiles of average ϵ and S_v during daytime and nighttime over 21–24 November 2011. Orange (black) curve indicates daytime (nighttime) ϵ, while green (cyan) curve demonstrates daytime (nighttime) S_v. Error bars denote the 95% bootstrap confidence limits.

4.3. Reduced Mixing Efficiency

From *Chameleon*'s independent measurements of χ_T (using fast thermistors) and ϵ (using shear probes, and following *Oakey* [1982], we estimate Γ by equating the turbulence diffusivity derived from the steady state, homogeneous, isotropic temperature variance evolution equation [*Osborn and Cox*, 1972] with that derived from the similar equation for turbulent kinetic energy [*Osborn*, 1980]: $\Gamma = N^2 \chi_T / 2\epsilon T_z^2$. Daytime values of Γ between 55 m and 85 m were 0.1–0.2 (Figure 11, orange curve), not significantly different from what has been found elsewhere in open ocean conditions [*Moum*, 1996a; *Gregg et al.*, 1986]. From nighttime profiles dominated by ichthyogenic turbulence (black curve), Γ is <0.02, i.e., smaller by an order of magnitude than the usual value. This occurs specifically because the ratio χ_T/ϵ is proportionately smaller within the fish aggregations.

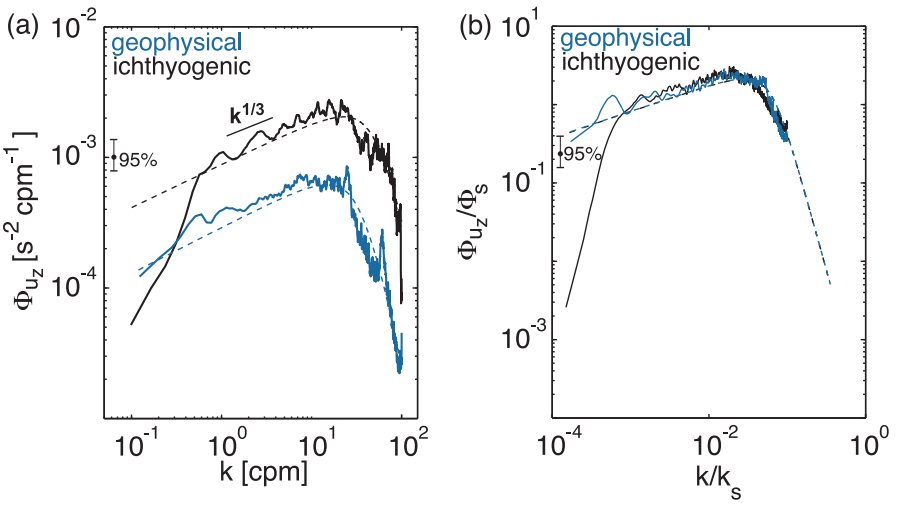

Figure 9. Shear spectrum for geophysical (blue; $1\times10^{-7} < \epsilon < 5\times10^{-7}$; $S_v < -52$ dB) and ichthyogenic (black; $9\times10^{-7} < \epsilon < 3\times10^{-6}$; $S_v > -45$ dB) turbulence. Each spectrum is an average of 46 individual spectra computed from shear probe measurements between 55 and 85 m during 21–24 November 2011. Dashed line indicates the universal spectrum, and error bars denote the 95% confidence interval. (a) Dimensionalized spectrum. Slope of inertial subrange is noted. (b) Nondimensionalized spectrum. $\Phi_s = (\epsilon/\nu^5)^{(1/4)}$. $k_s = (\epsilon/\nu^3)^{(1/4)}$. ν is viscosity of seawater.

5. Discussion

5.1. Behaviors and Characteristics of the Biological Aggregations

Although we make some comparisons here to studies that refer to fish schools, we have avoided the term "schools" as it connotes a specific behavior. Rather we use the more generic term "aggregation."

We have described the nighttime impact of biological aggregations on acoustic and turbulence measurements acquired from the ship. Acoustic scatterers believed to be fish aggregations peak at night and are concentrated toward the aft end of the ship, or downstream of the ship relative to the current. In the only comparable study we know of, *Plimpton et al.* [1997] observed contamination of velocity measurements by fish below an ADCP looking downward from a surface buoy. Nearly continuous month-long (and longer) aggregations caused high acoustic backscattering that biased ADCP estimates toward 0 m s^{-1} when compared to fixed-point measurements on the mooring cable below. In addition, the offending acoustic scatterers peaked in daylight hours and were found upstream of the mooring cable. *Plimpton et al.* [1997] attributed the aggregate scattering to tuna, which tend to stay upstream of FADs, according to *Holland* [1990]. This differs from our observations of nighttime fish aggregations found downstream of the ship. The observations of vertical and horizontal movements of tuna made by *Holland* [1990] and *Hoolihan et al.* [2014] indicate nighttime surfacing, consistent with results reported here but not with the *Plimpton et al.* [1997] observations. We have suggested why

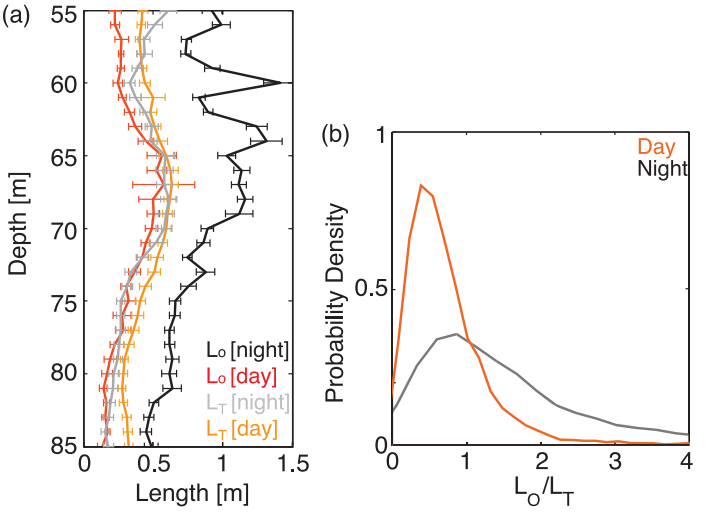

Figure 10. (a) Daytime and nighttime vertical profiles of average Ozmidov (L_O) and Thorpe (L_T) scales between 21 and 24 November 2011. Error bars indicate the 95% bootstrap confidence limits. (b) Probability distribution functions of $L_{OT} = L_O/L_T$ at nighttime and daytime from 55 to 85 m and between 21 and 24 November 2011.

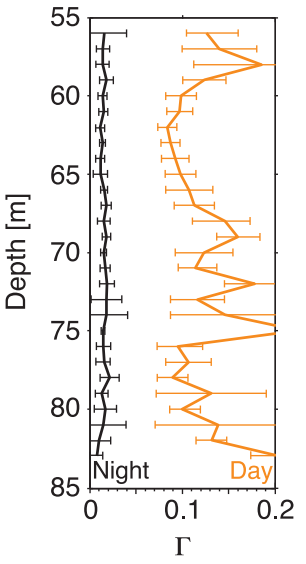

Figure 11. Daytime and nighttime vertical profiles of average mixing efficiency, Γ, during 21–24 November 2011. Error bars denote the 95% bootstrap confidence limits of daytime (orange) and nighttime (black) mean values.

the aggregates might be found aft of the ship in the light required for deck operations and why they might surface at night to feed on the surfaced zooplankton illuminated by the deck lights. Certainly, there are different factors between these two examples that are responsible for the differing behaviors.

The aggregation composition is uncertain as no net tows were performed. However, tuna were routinely observed during our experiment and likely responsible for much of the signal. Small fishing boats occasionally approached our vessel to sell recently caught tuna but were discouraged by ship's officers wary of uncontrollable personnel on board (pirates). Moreover, the scatterers were apparently able to swim against a current as fast as 1.5 m s^{-1} in order to keep up with the ship. This is a speed that zooplankton or smaller fish cannot achieve *Genin et al.* [2005]. Nighttime values of S_v varied from −55 to −35 dB, a range which *Lavery et al.* [2007] identified as inherent backscattering strength for fish. Tuna are fast swimmers, and dense populations have been previously recorded in the tropical Indian Ocean, particularly within the region where the ship was stationed [*Stéquert and Marsac*, 1989].

Tuna and other pelagic fish are commonly attracted to floating objects. *Røstad et al.* [2006] suggested that noise from the vessel engine and propeller may attract fish. This does not explain our nocturnal aggregations, because the propeller operated at all times of the day. An alternative explanation is that stern deck lights, turned on at night throughout the observational period, might have helped fish locate prey that would otherwise have been invisible in the absence of sunlight.

Diel vertical migration (DVM) of zooplankton involves dusk ascent to feed and dawn descent to evade predation. Because the antipredation function of nocturnal feeding is defeated by the deck lights, we speculate that DVM might partially explain fish aggregating below the vessel. Daily composites of S_v over depths of 100–350 m for the period 21–23 November, computed from echo intensity averaged over all beams of 75 kHz shipboard ADCP, revealed the daily ascent and descent of the associated deep scattering layers. The trajectory of the dominant scattering layer (there are more than one) is noted by the data points in Figures 12d and 12e. These time-dependent trajectories are reasonably represented by curves of the form $depth = a + be^{c(t-t_o)}$, where t_o is the time when the scattering layer starts to ascend or descend. Values for ascent and descent are noted in the caption to Figure 12, with time t in units of hours. The fitted trajectories are represented by the dashed gray curves in Figures 12d and 12e. The ascent and descent speeds of the scattering layers are shown by the red curves in Figures 12d and 12e, which is the time derivative of the trajectories. These speeds of 1–5 cm s^{-1} are roughly consistent with zooplankton swimming speeds.

Kunze et al. [2006] reported increased turbulence within migrating acoustic layers, which they suggested may mix nutrient-rich water upward. However, our measurements detected no increase in ϵ associated with the vertical migration of deep scattering layers below 90 m; ϵ within the layers was not different from background values (Figure 12c). This could be due to differences in species or population densities of turbulence-generating predators between the coastal inlet example sampled by *Kunze et al.* [2006] and the open ocean condition discussed here. This observation also does not rule out biogenic vertical water transport by means other than turbulent mixing, e.g., *Katija* [2012]. The surface arrival of the deep scattering layers coincides almost precisely with the large increase in S_v above 100 m and increased ϵ in the 50–80 m depth range, presumably due to the coincident arrival of fish. The descent of the deep scattering layer coincides with the simultaneous disappearance of high S_v in the upper 100 m and high ϵ in the 50–80 m depth range. When the scattering layer descends, the fish depart from the site.

5.2. Ichthyogenic Turbulence Characteristics

The characteristics of ichthyogenic turbulence are unique. Results from direct measurements in the ocean's main thermocline [*Moum*, 1996b] and from turbulence simulations of low Reynolds number instabilities

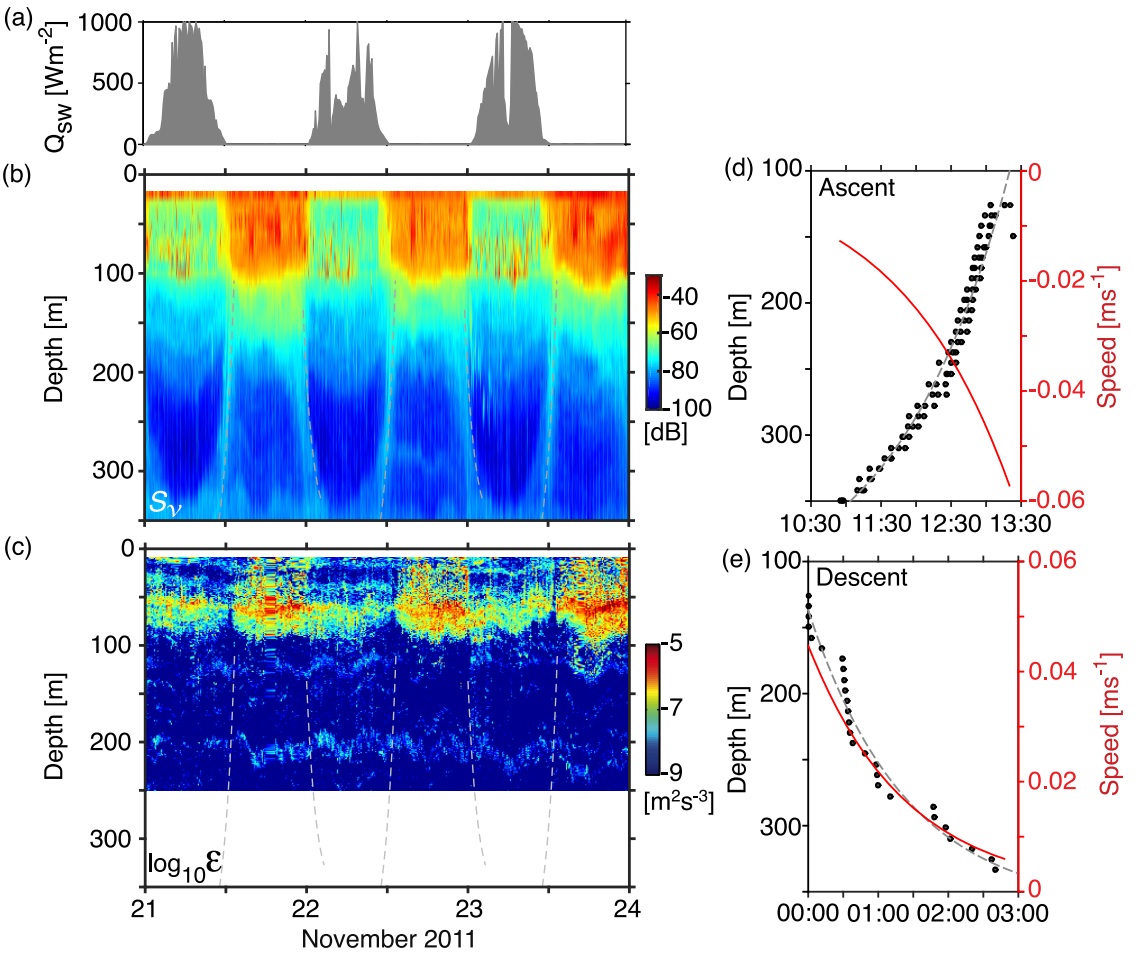

Figure 12. Time series of (a) Q_{SW}, (b) S_v from the R/V *Revelle* ADCP (75 kHz), and (c) ϵ during the period 21–23 November 2011. (d) Time series of S_v maxima delineating the nighttime ascent trajectory of a deep scattering layer from 350 to 120 m depth. Maxima defined from the data are represented by the black dots; the gray line represents the fit $depth = 430.6 - 77.6e^{0.6(t-11)}$ with *depth* in meters and time, *t* in hours. The red line is the derivative of the fit to the ascent trajectory, representing the ascent speed of the layer. (e) As in Figure 12d but representing the descent of the deep scattering layer at dawn, $depth = 362.3 - 225.5e^{-0.7t}$. Ascent and descent trajectories are echoed in Figures 12b and 12c as the dashed gray lines.

allowed to evolve from an initial stratified shear instability through growth, turbulence and final buoyancy suppression [*Smyth et al.*, 2001] have shown that the vertical dimension of turbulent patches is typically more than 10 × L_T. Figure 10 therefore suggests that the vertical dimension of the geophysical-scale instabilities is 5–7 m. This is significantly greater than the dimension that defines the observed low wave number cutoff of spectra (Figure 9a) we have identified with high S_v, roughly 1–2 m. This presumed vertical scale is also significantly greater than the scale of fish observed in the area during the experiment. The spectral forms in Figure 9 argue for small-scale isotropy (that is, isotropy at high wave numbers). The major distinction between the two spectra is the low wave number departure from the inertial subrange in ichthyogenic turbulence, indicative of low Re turbulence found in the lab and in numerical simulations but rarely in turbulence generated at geophysical scales.

Nighttime values of L_O, values we have associated with ichthyogenic turbulence, are 2–3 × L_T. This unusually large ratio conflicts with the observations of *Dillon* [1982] and many others, which show $L_O = L_T$ to within a few tens of percent in mechanically generated turbulence. In random samples of turbulent patches in the main thermocline at unknown stages of evolution [*Moum*, 1996b], occurrences of $L_O/L_T > 2$ represent only ∼1% of the observations. Laboratory measurements of grid-generated stratified turbulence confirm that $L_O \approx L_T$ [*Itsweire*, 1984]. Turbulence simulations [*Smyth et al.*, 2001] show small values of L_O/L_T at early stages of evolving instabilities, before the instabilities become fully turbulent. As turbulence develops, the ratio approaches ∼1. At the other extreme, large values of L_O/L_T are associated with large scale convective (rather than mechanically generated) overturns (B. D. Mater et al., Biases in Thorpe scale estimates of

turbulence dissipation. Part I: Assessments from large-scale overturns in oceanographic data, submitted to *Journal of Physical Oceanography*, 2014). Besides being much larger than values characteristic of mechanically generated geophysical turbulence, the nighttime ratio $L_O/L_T = 2$–3 observed here is statistically much larger than our own estimates made during daytime when fish were absent.

The large value of L_O/L_T for ichthyogenic turbulence is not unexpected, because fish inject turbulent kinetic energy much more rapidly than the usual geophysical instabilities, and at scales too small to be influenced by stratification. To see this, suppose that the turbulent dissipation rate immediately in the wake of a swimming fish is given by the inviscid scaling

$$\epsilon = C_\epsilon u^3/\ell, \tag{3}$$

in which ℓ and u are the length and velocity scales of the energy-containing eddies, presumably related to the size and swimming velocity of the fish. Estimates of the constant C_ϵ vary but are generally $O(1)$ [e.g., *Smyth et al.*, 1997]; for the present argument $C_\epsilon = 1$ suffices. This estimate for ϵ neglects the effects of stratification, but we can justify that neglect retroactively by computing the Ozmidov scale and comparing it with ℓ:

$$L_O/\ell = (u/\ell N)^{3/2}. \tag{4}$$

For a fish of height 0.1 m swimming at 1 m s^{-1} in water with $N = 10^{-2}$ s^{-1}, (4) gives $L_O/\ell = 3\times10^4$. While fish height and swimming speed are likely to be crude estimates of the turbulent length and velocity scales, it is clear that $L_O/\ell \gg 1$ in the immediate wake of the fish, i.e., turbulence is far too intense to feel the effect of stratification [and the use of (3) is justified]. The broad range of scales implied by this ratio provides support for the assumptions of stationarity, homogeneity, and isotropy that underlie our estimate of ϵ (section 2.2). As the wake spreads, ℓ increases and u decreases; hence, L_O/ℓ decreases rapidly, eventually approaching $O(1)$ as stratification arrests the spreading. To estimate the wake thickness when $L_O/\ell = 1$, we assume that the product $u\ell^2$ is constant (consistent with continuity in a self-similar wake), in which case L_O/ℓ decreases in proportion to $\ell^{-9/2}$. Based on this, L_O/ℓ decreases to 1 when the thickness of the wake has increased by a factor 10, to about 1 m in the present example. In this view, it is not surprising that $L_O/L_T > 1$ and is occasionally even $\gg 1$ (Figure 10b). The results are therefore consistent with the interpretation that our instruments are sampling different stages of spreading fish wakes.

The low mixing efficiency of ichthyogenic turbulence is associated with small χ_T relative to ϵ. This property suggests that the intense turbulence in fish wakes rapidly erases local temperature gradients, so that χ_T drops to zero in the wake, while viscous dissipation continues until turbulent motions cease.

An implication of this reduced mixing efficiency is that, if fish were present at the mooring, our moored measurements of ϵ_χ could underestimate the true dissipation rate, because ϵ_χ is inversely proportional to Γ and we assume $\Gamma = 0.2$ for that calculation. In the interpretation of Figure 2c, for example, we have assumed that dissipation is lower at the mooring than at the ship because fish are absent. But low-efficiency ichthyogenic turbulence could lead, erroneously, to the same low value of ϵ_χ, i.e., fish could be present but invisible due to their low mixing efficiency. Our original interpretation holds, however, for three reasons. (1) The moored ADCP did not show the day-night difference that fish would generate (Figure 4a). (2) With the onset of strong winds on November 24th, the moored ADCP detected a smooth acceleration and deepening of the surface current, just as one would expect (compare Figures 2a and 2b), with no discontinuity associated with the change in S_v (Figure 2e). (3) There was no day-night difference in dissipation measured at the mooring (Figure 7). We conclude that ichthyogenic turbulence was not observed at the mooring because aggregations were not present at the mooring during our observations.

6. Conclusion

We have examined the effects of fish, swimming steadily to keep pace with a ship under power, on both current measurements and turbulence. Our main conclusions are as follows.

Ichthyogenic effects were local to the ship; there was no evidence of such effects at a mooring 1 km away. The evidence suggests that fish were attracted by nocturnally feeding zooplankton illuminated by the deck lights.

Swimming fish had a significant effect on acoustic velocity measurements. Those effects proved to be identifiable via shipboard ADCP in the form of a sporadic reduction of the measured speed. Using a combination

of shipboard and moored ADCPs, we have quantified the ichthyogenic fraction of the ADCP signal; in this case 20–30%.

Swimming vigorously, the fish generated turbulence at levels (measured by the kinetic energy dissipation rate) comparable to those resulting from geophysical flow instabilities. Compared with geophysical turbulence, turbulence in fish wakes represents a large concentration of turbulent kinetic energy in a small space. As a result, this ichthyogenic turbulence exhibits three measureable characteristics that distinguish it from geophysical turbulence: (1) Eddies on scales greater than about 1 m are absent from the shear spectrum. (2) Eddies are too small to be significantly affected by density stratification ($L_T \ll L_O$). (3) Mixing efficiency (Γ) is small, i.e., turbulent energy is mostly converted to very small quantities of heat via viscous dissipation.

In transects through fish aggregations apparently unaffected by the presence of the ship, *Gregg and Horne* [2009] observed ichthyogenic turbulence with properties very similar to those listed above. We infer that these properties are characteristic of a wide range of biophysical regimes.

Low mixing efficiency, together with the fact that only a small fraction of the stratified ocean is occupied by fish aggregations, suggests that the ichthyogenic contribution to ocean mixing by horizontally swimming fish is negligible.

Acknowledgments
Thanks to Ray Kreth, Mike Neeley-Brown, Alexander Perlin, Aurelie Moulin, Elizabeth McHugh, and Rita Brown for helping with data collection and initial data processing. Constructive comments from two anonymous reviewers are greatly appreciated. Funding for this project has been provided by the Office of Naval Research (N001-10-7-2098), the National Science Foundation (grants OCE1030772, OCE1129419, OCE1336752, and OCE1059055). Data from the DYNAMO project are archived at https://www.eol.ucar.edu/field projects/dynamo.

References

Dillon, T. (1982), Vertical overturns: A comparison of Thorpe and Ozmidov length scales, *J. Geophys. Res.*, *87*(C12), 9601–9613.
Farmer, D. D., G. B. Crawford, and T. R. Osborn (1987), Temperature and velocity microstructure caused by swimming fish, *Limnol. Oceanogr.*, *32*(4), 978–983.
Genin, A., J. S. Jaffe, R. Reef, C. Richter, and P. J. Franks (2005), Swimming against the flow: A mechanism of zooplankton aggregation, *Science*, *308*(5723), 860–862.
Gregg, M., E. d'Asaro, T. Shay, and N. Larson (1986), Observations of persistent mixing and near-inertial internal waves, *J. Phys. Oceanogr.*, *16*(5), 856–885.
Gregg, M. C., and J. K. Horne (2009), Turbulence, acoustic backscatter, and pelagic nekton in Monterey Bay, *J. Phys. Oceanogr.*, *39*(5), 1097–1114.
Holland, K. N. (1990), Horizontal and vertical movements of yellowfin and bigeye tuna associated with fish aggregating devices, *Fish. Bull.*, *88*, 493–507.
Hoolihan, J., R. Wells, J. Luo, B. Falterman, E. Prince, and J. Rooker (2014), Vertical and horizontal movements of yellowfin tuna in the Gulf of Mexico, *Mar. Coastal Fish.*, *6*(1), 211–222.
Itsweire, E. C. (1984), Measurements of vertical overturns in a stably stratified turbulent flow, *Phys. Fluids*, *27*(4), 764–766.
Katija, K. (2012), Biogenic inputs to ocean mixing, *J. Exp. Biol.*, *215*(6), 1040–1049.
Kunze, E., J. F. Dower, I. Beveridge, R. Dewey, and K. P. Bartlett (2006), Observations of biologically generated turbulence in a coastal inlet, *Science*, *313*(5794), 1768–1770.
Lavery, A. C., P. H. Wiebe, T. K. Stanton, G. L. Lawson, M. C. Benfield, and N. Copley (2007), Determining dominant scatterers of sound in mixed zooplankton populations, *J. Acoust. Soc. Am.*, *122*(6), 3304–3326.
Lorke, A., and W. N. Probst (2010), In situ measurements of turbulence in fish shoals, *Limnol. Oceanogr. Methods*, *55*(1), 354–364.
McPhaden, M. J., G. Meyers, K. Ando, Y. Masumoto, V. S. N. Murty, M. Ravichandran, F. Syamsudin, J. Vialard, L. Yu, and W. Yu (2009), RAMA: The research moored array for African–Asian–Australian monsoon analysis and prediction, *Bull. Am. Meteorol. Soc.*, *90*(4), 459–480, doi: 10.1175/2008BAMS2608.1.
Moum, J., and J. Nash (2009), Mixing measurements on an equatorial ocean mooring, *J. Atmos. Oceanic Technol.*, *26*(2), 317–336.
Moum, J., M. Gregg, R. Lien, and M. Carr (1995), Comparison of turbulence kinetic energy dissipation rate estimates from two ocean microstructure profilers, *J. Atmos. Oceanic Technol.*, *12*, 346–366.
Moum, J. N. (1996a), Efficiency of mixing in the main thermocline, *J. Geophys. Res.*, *101*(C5), 12,057–12,069.
Moum, J. N. (1996b), Energy-containing scales of turbulence in the ocean thermocline, *J. Geophys. Res.*, *101*(C6), 14,095–14,109.
Moum, J. N., et al. (2014), Air-sea interactions from westerly wind bursts during the November 2011 MJO in the Indian Ocean, *Bull. Am. Meteorol. Soc.*, *95*, 1185–1199, doi:10.1175/BAMS-D-12-00225.1.
Nasmyth, P. W. (1970), Oceanic turbulence, PhD thesis, Univ. of B. C., Vancouver, Canada.
Oakey, N. (1982), Determination of the rate of dissipation of turbulent energy from simultaneous temperature and velocity shear microstructure measurements, *J. Phys. Oceanogr.*, *12*(3), 256–271.
Osborn, T. (1980), Estimates of the local rate of vertical diffusion from dissipation measurements, *J. Phys. Oceanogr.*, *10*(1), 83–89.
Osborn, T. R., and C. S. Cox (1972), Oceanic fine structure, *Geophys. Astrophys. Fluid Dyn.*, *3*(1), 321–345.
Plimpton, P. E., H. P. Freitag, and M. J. McPhaden (1997), ADCP velocity errors from pelagic fish schooling around equatorial moorings, *J. Atmos. Oceanic Technol.*, *14*(5), 1212–1223.
Røstad, A., S. Kaartvedt, T. A. Klevjer, and W. Melle (2006), Fish are attracted to vessels, *ICES J. Mar. Sci. J. Cons.*, *63*(8), 1431–1437.
Rousseau, S., E. Kunze, R. Dewey, K. Bartlett, and J. Dower (2010), On turbulence production by swimming marine organisms in the open ocean and coastal waters, *J. Phys. Oceanogr.*, *40*(9), 2107–2121, doi:10.1175/2010JPO4415.1.
Smyth, W., P. Zavialov, and J. Moum (1997), Decay of turbulence in the upper ocean following sudden isolation from surface forcing, *J. Phys. Oceanogr.*, *27*(5), 810–822.
Smyth, W., J. Moum, and D. Caldwell (2001), The efficiency of mixing in turbulent patches: Inferences from direct simulations and microstructure observations, *J. Phys. Oceanogr.*, *31*(8), 1969–1992.
Stéquert, B., and F. Marsac (1989), Tropical tuna: Surface fisheries in the Indian Ocean, *FAO Fish. Tech. Pap. 282*, Food and Agricultural Organization, Rome.
Yoneyama, K., C. Zhang, and C. N. Long (2013), Tracking pulses of the Madden–Julian Oscillation, *Bull. Am. Meteorol. Soc.*, *94*(12), 1871–1891, doi:10.1175/BAMS-D-12-00157.1.